δ-function-shaped Sb-doping profiles in Si(001) obtained using a low-energy accelerated-ion source during molecular-beam epitaxy

W.-X. Ni, G. V. Hansson, J.-E. Sundgren, and L. Hultman
Department of Physics, Linköping University, S-581 83 Linköping, Sweden

L. R. Wallenberg
Chemical Center, University of Lund, P.O. Box 124, S-221 00 Lund, Sweden

J.-Y. Yao
Department of Physics, Chalmers University of Technology, S-412 96 Göteborg, Sweden

L. C. Markert and J. E. Greene
Department of Material Science, The Coordinated Science Laboratory and The Materials Research Laboratory, University of Illinois, 1101 West Springfield Avenue, Urbana, Illinois 61801
(Received 1 April 1992)

Two-dimensional (2D) buried δ-function-shaped Sb-doping profiles have been obtained in Si using a low-energy accelerated Sb-ion source during molecular-beam epitaxy. A combination of secondary-ion mass spectrometry (SIMS), capacitance-voltage (C-V) measurements, and cross-sectional transmission electron microscopy (XTEM) was used to investigate dopant distributions and to determine profile widths. The 2D-sheet Sb-doping concentration N_{Sb}, obtained by integrating SIMS δ-doping profiles in samples grown with substrate temperature $T_s = 620\,^{\circ}C$ and Sb-ion acceleration potentials $V_{Sb} = 200$ and 300 V, was found to vary linearly with the product of the Sb-ion flux and the exposure time (i.e., the ion dose) over the N_{Sb} range from 5×10^{12} to 2×10^{14} cm^{-2}. The full width at half maximum (FWHM) concentration of δ-doping profiles in Si(001) films was less than the depth resolution of both SIMS and C-V measurements (~ 10 and 3 nm, respectively). High-resolution XTEM lattice images show that the FWHM was ≤ 2 nm. This is consistent with dopant incorporation simulations, based upon a multisite transition-state dopant incorporation model, which show that accelerated-beam dopant species are trapped in near-surface substitutional sites with atomic mobilities between those of surface and bulk atoms. Dopant surface segregation during growth is strongly suppressed, and the dopant distribution is determined primarily by the straggle in ion trapping distributions. The present results are compared with profile broadening observed in δ-doped layers obtained by solid-phase epitaxy of amorphous Si containing a buried Sb layer.

I. INTRODUCTION

Semiconductor structures with buried δ-function-shaped doping profiles have attracted considerable interest since they exhibit promising properties, e.g., quantum size effects,[1-3] that can be used for optimizing conventional semiconductor devices or producing novel device structures.[1] The term "δ doping" implies that the dopant atoms are distributed two-dimensionally in a single lattice plane.[4] In practice, however, the term δ doping is applied to very thin doped regions with widths less than a few nanometers. δ-doped structures have been grown in III-V semiconductors using molecular-beam epitaxy (MBE).[1] However, thermal coevaporation doping during Si MBE gives rise to severe problems due to surface segregation.[5] Sb, which is the most commonly used n-type dopant in Si MBE, exhibits both a low incorporation probability and strong surface segregation.[6] The latter results in an accumulation of Sb atoms on the surface during deposition and, consequently, severe smearing of the doping profile.

Synthesis of δ-doped profiles in MBE Si requires the use of novel doping techniques. Zeindl *et al.*[2] have used solid-phase epitaxy (SPE). In their experiments, they interrupted film growth, cooled the sample down to ambient temperature where the dopant incorporation probability is unity and surface segregation is minimized, and then deposited thermal Sb to obtain a surface coverage of $\sim 10^{13}$ cm^{-2}. A 3-nm-thick amorphous Si layer was then deposited on top of the Sb and the structure was crystallized by SPE at a temperature of 700 °C. Cross-sectional transmission electron microscopy (XTEM) studies showed that the doped layer was $\sim 2-3$ nm thick. This technique, however, suffers from several problems. First, it is difficult to precisely and reproducibly control small thermal Sb fluxes, and hence δ-doping concentrations, which are exponentially dependent upon the effusion cell temperature. Second, there is an increased risk of contaminant absorption at ambient temperature as well as of precipitation and defect formation during crystallization

of the amorphous Si layer. All of these effects lead to increased carrier scattering at the doped-undoped layer interface, and result in lower carrier mobilities.

The SPE δ-doping method was modified by van Gorkum, Nakagawa, and Shiraki.[7] They dosed Si surfaces at temperatures between 500 °C and 700 °C with a constant Sb thermal flux to reach a saturated surface coverage of Sb, and then annealed the samples at 750 °C for sufficient times to obtain the desired Sb coverage by thermal desorption before depositing the amorphous Si overlayer. This provided better control of the two-dimensional (2D)-sheet doping concentration, N_{Sb}^{2D}.

We have taken a different approach for synthesizing δ-doped layers by utilizing low-energy ion-beam doping.[8,9] The advantage of this method is that dopant deposition can be carried out at the Si growth temperature, while the dopant distribution will be restricted to a thin layer determined primarily by the straggle in the ion-trapping distribution. Extensive studies of low-energy Sb ion doping during MBE growth of thick Si films have been reported previously.[10] It was shown that a unity incorporation probability and complete electrical activation[11] can be obtained over a wide range in ion energy and film growth temperature. In Sb-ion δ-doped layers, quantum confinement has been observed by low-temperature tunneling current measurements,[3] and a metal Schottky gate field-effect transistor with improved channel conductance has also been fabricated with a Sb-ion δ-doped layer.[12]

In this paper, we present an extensive study of the growth and characterization of Sb δ-doped structures, obtained using a low-energy Sb-ion source operated with acceleration potentials ranging from 50 to 500 V during Si MBE. Secondary-ion mass spectrometry (SIMS), capacitance-voltage (*C-V*) measurements, and cross-sectional transmission electron microscopy (XTEM) were used to investigate dopant distributions and to determine depth profiles. Well-controlled δ-doping profiles with very narrow widths (≤ 2 nm) and no degradation of the Si crystalline quality were achieved at a growth temperature T_s of 625 °C.

II. EXPERIMENTAL PROCEDURE

Si films containing δ-function-shaped Sb doping layers were grown on (001)-oriented Si substrates in a Vacuum Generators V-80 MBE system. Doping was carried out using an electron-impact, single-grid, low-energy ion source[10] providing an accelerated Sb ion beam ($V_{Sb}=50-500$ V). An electrostatic mirror deflector was used in order to remove neutral species. The dopant flux incident at the substrate was determined using a translatable Faraday cup. The extracted ion beam from this source, characterized using charge-to-mass ratio measurements,[10] contains Sb^+, Sb_2^+, and Sb_4^+ ions, each with its own implantation distribution. The relative contributions of the different species to the ion current have been reported in Ref. 10 and the average number of Sb atoms per unit charge is 2.2 atoms/*e*.

n-type substrates with a resistivity $\rho \leq 0.02$ Ω cm were used for *C-V* measurements, while *p*-type substrates with $\rho \approx 8$ Ω cm were used for all other measurements. The details of the sample preparation and cleaning have been given in Ref. 10. The δ-doped layers were obtained using the following procedure. After growth of a 250-nm-thick Si buffer layer at $T_s=750$ °C, the Si deposition was interrupted while the sample surface was exposed, typically at $T_s \approx 625$ °C, to the low-energy Sb-ion beam. The exposure time was chosen such that the desired sheet doping concentration was obtained for a given ion flux. An undoped Si cap layer, 10–100 nm thick, was then grown at the same temperature.

As a comparison, a few Sb δ-doped samples were also prepared using the SPE method described in Ref. 2. In this case, the Sb flux was supplied from a standard effusion cell which was calibrated using a quartz-crystal monitor. For high exposures, Sb surface coverages were checked by Auger electron spectroscopy (AES).

The δ-doped layers were examined by SIMS, using a Cameca IMS-3F microprobe system operated with a Cs^+ primary ion beam, in order to determine dopant distributions and total incorporated dopant concentrations. Sb-ion-implanted wafers with known distributions were used as standards to convert SIMS intensity to Sb concentration units. Sb sheet doping concentrations were obtained by integrating the area of measured SIMS intensity peaks.[13] In these measurements, the potential difference between the primary ion source and the secondary ion detector was maintained at -12.5 keV. The impact energy of the primary ions at the sample depended upon the polarity of the secondary ions detected. For positive secondary ions, the impact energy was 8 keV, while for negative ions it was 17 keV. The results presented in this paper were obtained using positive secondary ions in order to obtain the best depth resolution.

Pt Schottky contacts (diameter of 0.05 cm) were evaporated through a mask onto Si cap layers in order to use high-frequency (1-MHz) *C-V* measurements to probe buried δ-doped layers. The *C-V* setup consists of a Boonton capacitance meter with a voltage ramp generator and regulating circuit. XTEM studies of δ-doped layers were performed using a Philips EM 400T electron microscope operated at 120 kV, $\mathbf{g}_{311}$ weak-beam images were obtained using a JEOL 2000FX microscope at 200 keV, and high-resolution lattice images were obtained using a JEOL 4000EX microscope at 400 kV. (011)-oriented cross sections of the samples were prepared for TEM by mechanical thinning followed by ion milling.

III. MODEL CALCULATIONS OF δ-DOPING PROFILES

Coevaporated thermal Sb doping during Si MBE results in strong surface segregation and dopant accumulation. Our recent studies have shown that at $T_s=600$ °C–700 °C, the steady-state fraction of Sb in the surface adlayer is four to five orders of magnitude higher than the bulk fraction.[13] The surface accumulation layer then serves as a source for doping of subsequently grown buffer layers even after the incident dopant flux has been interrupted. Thus doping profiles become seriously broadened and smeared out. However, it has been demonstrated[10] that low-energy ion-beam doping can effectively suppress the dopant surface segregation and

produce abrupt doping profiles. The Sb ions, shallowly implanted by the low acceleration energy, are trapped in near-surface sites with atomic mobilities intermediate between those of Sb atoms in surface and bulk sites.

The incorporation behavior of low-energy accelerated dopants is very different from that of a thermally evaporated dopant beam at typical growth temperatures. This can be demonstrated by *in situ* AES measurements as the dopant layers are overgrown by Si. Figure 1 shows the intensity of the 454-eV Sb(*MNN*) Auger transition, normalized to the intensity obtained from the surface immediately after a $V_{Sb}=300$ eV ion-beam exposure, versus the thickness of the Si cap layer which was grown at 600 °C. The exponential decay of the Sb(*MNN*) peak intensity indicates that the Si cap grew layer by layer with no Sb floating on top of the growth surface. A mean escape depth value of 0.97 nm for Sb(*MNN*) Auger electrons through Si was obtained from the slope of the decay curve. For contrast, Fig. 1 also shows AES measurements from a sample with a thermally evaporated Sb overlayer, on top of which a Si cap layer was grown at 600 °C. In this case, there is only a very small decrease in the Sb Auger intensity during the initial stages of Si-layer growth, indicating that Sb atoms are following the growth surface. These observations are in good agreement with our model calculations, and support the interpretation that dopant segregation occurs primarily through near-surface sites with low kinetic barriers for atomic motion. However, if dopant atoms can be trapped into deeper sites with bulklike atomic surroundings by, e.g., low-energy ion implantation, surface segregation is greatly decreased.

Calculations of dopant profiles, using a five-level multisite transition-state model,[10] have been carried out in order to explain the difference in the kinetics of thermal and accelerated dopant surface segregation and bulk incorporation. In this model, the time-dependent dopant concentration in atomic layer i can be computed by numerically integrating the following set of differential equations with the boundary condition that the flux of dopant atoms has been interrupted after an initial exposure at time $t=0$,

$$\frac{dn_1}{dt}=-\left[K_{\rm des}+r_{1,2}+\frac{1}{\tau}\right]n_1+r_{2,1}n_2\ , \tag{1a}$$

$$\frac{dn_i}{dt}=\left[r_{i-1,i}+\frac{1}{\tau}\right]n_{i-1}-\left[r_{i,i-1}+r_{i,i+1}+\frac{1}{\tau}\right]n_i+r_{i+1,i}n_{i+1}\ , \tag{1b}$$

$$\frac{dn_m}{dt}=\left[r_{m-1,m}+\frac{1}{\tau}\right]n_{m-1}-\left[r_{m,m-1}+\frac{1}{\tau}\right]n_m\ , \tag{1c}$$

where n_i is the dopant density in layer i ($i=1,2,\ldots,m$). τ is the time required for growth of one Si layer, $(a_0/4)R_{\rm Si}$, where a_0 is the Si lattice constant and $R_{\rm Si}$ is the Si growth rate. The calculations were truncated in the mth layer by setting $r_{m+1,m}n_{m+1}=r_{m,m+1}n_m$. $K_{\rm des}$ is the desorption coefficient, and the exchange rate r_{ij} between two adjacent sites is expressed as

$$r_{ij}=\begin{cases}\nu_{ij}n_i\exp\left[-\dfrac{E_i+\Delta H_{ij}^s}{kT_s}\right] & (j=i+1,\ i\geq 1)\\ \nu_{ij}n_i\exp\left[-\dfrac{E_i}{kT_s}\right] & (j=i-1,\ i\geq 2)\ ,\end{cases} \tag{2}$$

where ν_{ij} is a frequency factor, E_i is the energy barrier height, and ΔH_{ij}^s is the enthalpy difference between two adjacent sites. The detailed formalism of this model can be found in Ref. 10.

The major difference encountered when applying the model to coevaporation and accelerated ion doping is due to differences in the initial near-surface dopant atom distribution. Prior to the onset at $t=0$ of the Si cap layer position, a fraction of a monolayer of Sb is deposited either on the surface (thermal doping case), i.e., $n_1(t=0)=\Theta_d$, $n_i(t=0)=0$ ($1<i\leq m$), or in near-surface sites with a distribution described by the sum of three Gaussian functions (low-energy ion doping) accounting for an ion beam consisting of three different ion species.

Equations (1a)–(1c) are solved numerically using a Runge-Kutta method to obtain the final depth distribution of dopant atoms.[10] In the present study, the first 45 layers below the surface were involved in the calculations, but only the top five sites had barrier heights and/or potential energy minima different from bulk values.

Using the energy parameters obtained in Ref. 10 by fitting experimental incorporation probability data together with projected range and straggle values estimated from an extrapolation of high-energy implantation data,[14] Sb dopant profiles were computed for both thermal and ion-beam ($V_{\rm Sb}=0$, 100, 250, and 500 V) doping at $T_s=650$ °C. The results are summarized in Fig. 2. For thermal doping, only very small amounts of Sb are incorporated into the lattice. Most dopant atoms continuously

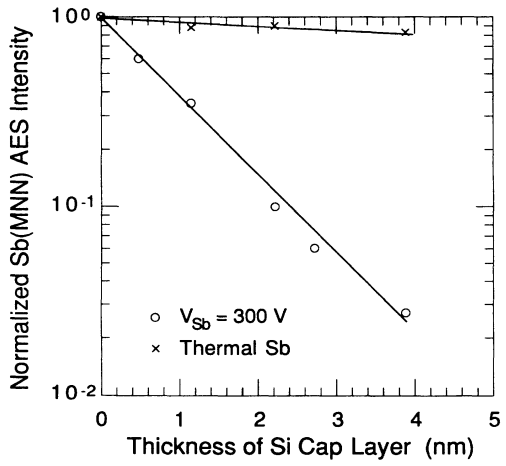

FIG. 1. Normalized peak-to-peak intensities of the 454-eV Sb(*MNN*) Auger transition vs the thickness of Si cap layers grown at 600 °C on Sb overlayers deposited on Si(001) substrates by either a 300-V accelerated-Si-ion beam (○) or a thermal Sb beam (×).

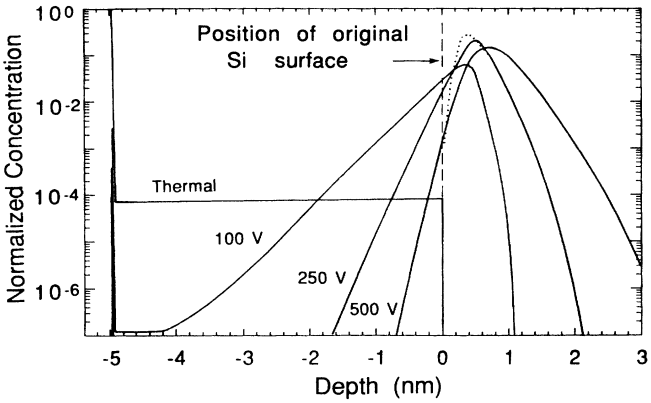

FIG. 2. Calculated Sb-dopant depth distributions in Si(001) for thermal doping and accelerated-ion doping with $V_{Sb}=100$, 250, and 500 V after growth of a 5-nm-thick Si overlayer. The vertical dashed line gives the position of the original Si substrate surface while the dotted curve shows the initial depth distribution of Sb implanted with $V_{Sb}=250$ V.

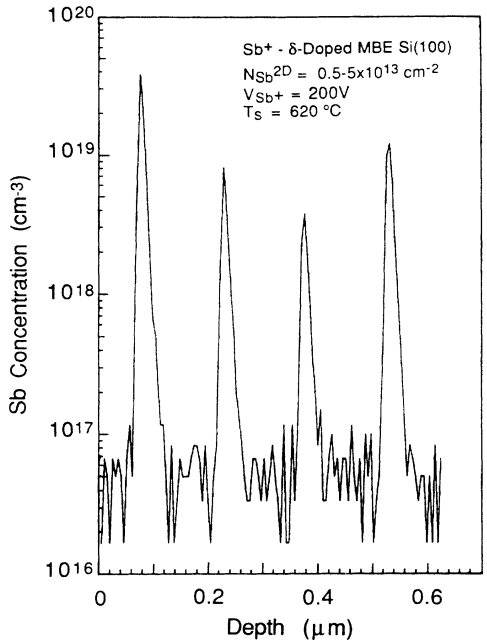

FIG. 3. SIMS profile through a Sb modulation δ-doped MBE Si film. The Sb-ion beam was accelerated using $V_{Sb}=200$ V and Sb sheet concentrations N_{Sb}^{2D} were varied from 5×10^{12} to 5×10^{13} cm^{-2}.

segregate to the growth surface. The resulting doping profile is thus completely smeared out with a high concentration in the surface layer (at the position ≈ -5 nm in Fig. 2). However, during the accelerated ion-beam exposures, surface segregation was strongly suppressed. The dotted curve of Fig. 2 shows that the dopant atom distribution, immediately after exposure to a 250-eV Sb-ion beam, has a full width at half maximum (FWHM) intensity of 0.45 nm. Only a very small fraction ($\leq 0.1\%$) of the Sb atoms end up at top surface sites for $V_{Sb}=250$ V and segregation is negligible at higher ion-acceleration energies. After a 5-nm-thick Si cap layer is grown at 625 °C, the 250-V profile is slightly broader than the implanted profile and the peak height is also decreased somewhat since there is still a small loss of dopant atoms towards the surface. However, there is almost no change in the FWHM (0.5 nm) and the width at 10% of the peak height is ~ 1.2 nm. Simulated profile broadening due to bulk diffusion during the growth of subsequent layers is negligible for $T_s \leq 700$ °C.

The exact shape of the dopant profiles depends strongly on the acceleration potential of the Sb-ion beam. For example, with $V_{Sb} \leq 100$ V, surface segregation is still strong, the Sb incorporation probability is low, and the profile is broadened and distorted to some degree. For $V_{Sb} > 200$ V, there is almost no surface segregation. However, as V_{Sb} increases, the ion straggle and the probability of residual ion damage increases. Thus, the optimum acceleration potential for producing δ-doped layers by a Sb-ion beam is approximately 250 V, corresponding to an average energy per incident Sb atom of 120 eV.

IV. EXPERIMENTAL RESULTS AND DISCUSSION

A. SIMS measurements

Typical SIMS profiles, obtained using 8-keV Cs^+ primary ions and $(SbCs)^+$ secondary ions, of δ-doped layers grown at $T_s=620$ °C with $V_{Sb}=200$ V for different Sb-ion exposure times are shown in Fig. 3. The FWHM values of the profiles, ≈ 12 nm, are limited by ion etching artifacts including collisional and forward recoil mixing during profiling.[15] The true FWHM values are expected to be much smaller and closer to those of the calculated profiles shown in the previous section. The slope of the leading edge of the measured profiles (≈ 3.6 nm/concentration decade in Fig. 3) was always much sharper than that of the tailing edge (≈ 14 nm/concentration decade), due to the forward-to-backward asymmetry of the primary-ion collision cascade.

Using bulk Si wafers with known Sb-ion-implanted profiles as standards, the sheet doping concentration N_{Sb}^{2D} in the δ-doped profiles can be obtained from the total integrated area under SIMS profiles such as those shown in Fig. 3. N_{Sb}^{2D} values from δ-doped profiles grown at $T_s=620$ °C with $V_{Sb}=200$ and 300 V were determined, and compared with the ion dose D_{Sb^+}. The results show that N_{Sb}^{2D} and D_{Sb^+} are proportional (within a 25% experimental error) with a ratio of unity for the sheet concentrations investigated between 4×10^{12} and 1.5×10^{14} cm^{-2}. This indicates that Sb-ion incorporation in a δ-doped layer during Si MBE is a first-order process in agreement with our previous Hall measurements,[16] which showed that Sb is incorporated into electrically active substitutional sites with essentially 100% probability for $V_{Sb}=100$ V and $T_s=620$ °C.

The incorporation probability σ_{Sb} of Sb ions in a δ-doped layer is dependent upon both the ion energy and the substrate temperature. As shown in Fig. 4 for

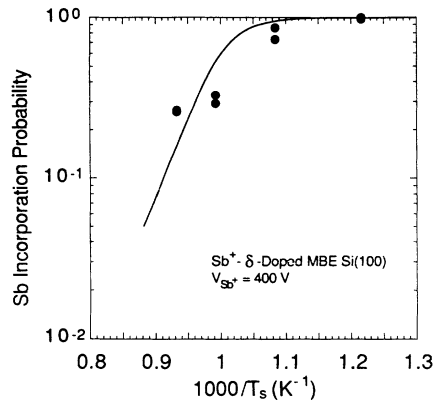

FIG. 4. The incorporation probability σ_{Sb} in Si(001) determined by SIMS measurements of Sb-ion δ-doped MBE Si as a function of substrate temperature T_s. $V_{Sb}=400$ V. The solid curve shows calculated results.

$V_{Sb}=400$ V, complete incorporation is only obtained for $T_s<650$ °C. As a comparison, the calculated incorporation probability of δ-doped Sb ions, using the above model, is also shown in Fig. 4 by a solid curve.

B. Capacitance-voltage (*C-V*) measurements

Room-temperature high-frequency *C-V* measurements were used to estimate the width, sheet concentration, and depth of δ-doped layers below the film surface. A typical carrier profile obtained from the *C-V* characteristics using standard equations based on the depletion approximation for an abrupt boundary[17] is shown in Fig. 5. The measurements were carried out on a Pt Schottky diode fabricated on a 50-nm Si-capped δ-doped layer grown at $T_s=650$ °C with $V_{Sb}=250$ V and $N_{Sb}^{2D}\approx 5\times10^{12}$ cm^{-2}. Both the position of the peak maximum, 52 nm, and the measured sheet concentration $N_{Sb}^{2D}=4.8\times10^{12}$ cm^{-2}, obtained from the peak area, in Fig. 5 agree well with expected values based upon film growth parameters. The

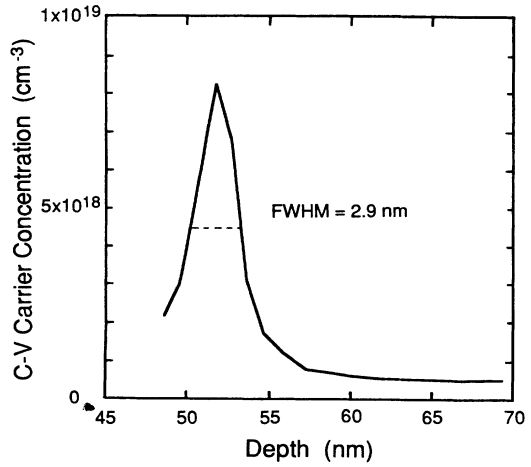

FIG. 5. *C-V* carrier concentration profile obtained from a Sb-ion δ-doped MBE Si film grown with $V_{Sb}=250$ V and $T_s=650$ °C. $N_{Sb}^{2D}=5\times10^{12}$ cm^{-2}.

FWHM of the *C-V* profile is 2.9 nm, which is a measure of the width of the distribution of electrons in the δ-doped layer. The corresponding width of the distribution of dopant atoms is necessarily much smaller. Starting from the calculated width of the dopant atom profile using the aforementioned dopant incorporation model (0.5 nm), it is possible to estimate an expected FWHM value of the *C-V* profile in the present case. Using a method proposed by Schubert and Ploog,[18] a quantum-mechanical calculation predicts a FWHM of 3.3 nm for the *C-V* profile measured on a 0.5-nm-wide distribution of Sb atoms.

It has been noted that in the *C-V* characteristics sometimes only the initial gradual drop of the high-frequency capacitance with applied negative voltage corresponding to the increasing thickness of the depletion layer in the near-surface region may provide useful information. In this region the reverse leakage current of the Schottky diode was low ($\lesssim5\times10^{-3}$ A cm^{-2}). An avalanche breakdown occurred as the diode was reverse biased by more than 3 V where the leakage current increased rapidly. There was also a rapid decrease in the capacitance for $V<-2.7$ V due to the onset of avalanche breakdown. Up to this limit, the electric field between the metal contact and the δ-doped layer was $\lesssim6\times10^{5}$ V cm^{-1}. The maximum amount of charge Q that can be depleted under these conditions was estimated from the definition of capacitance for an ideal parallel plate capacitor, $C=QA/(V+\Phi)$, where A is the area of the Schottky junction and Φ is the height of the surface band bending induced by the metal-Si contact, to be 5.3×10^{12} cm^{-2}. This value is in good agreement with similar estimates (3.5×10^{12} cm^{-2}) by van Gorkum, Nakagawa, and Shiraki[7] obtained from SPE-grown δ-doped layers. It is thus not meaningful to analyze *C-V* measurements on δ-doped samples with sheet concentrations larger than 5×10^{12} cm^{-2}.

C. TEM characterization

XTEM was used to examine δ-doped layers. A typical bright-field image from a (011)-oriented cross-section foil with a Sb δ-doped layer grown at $T_s=625$ °C with $V_{Sb}=250$ V and a Sb exposure to yield $N_{Sb}^{2D}=6\times10^{13}$ cm^{-2} is shown in Fig. 6. The measured width of the band of contrast is ~2 nm, which is in reasonable agreement with the calculated width of the dopant distribution over which the dopant atom concentration was > 10% of the peak value (1.2 nm in Fig. 2). The contrast observed at Sb δ-doped layers in XTEM micrographs has previous-

FIG. 6. Bright-field XTEM image of a Sb-ion δ-doped MBE Si(001) layer grown with $V_{Sb}=250$ V and $T_s=625$ °C. $N_{Sb}^{2D}=5\times10^{13}$ cm^{-2}.

ly been attributed to an increased scattering of the electron beam by the heavy dopant atoms.[2] Furthermore, no dislocation loops or other extended defects were observed, even far away from the δ-doped layer, which indicates no segregation of point defects. These results also imply that the surface damage induced by ion doping is very small.

In order to rule out the possibility that the observed contrast band in Fig. 6 is partly due to contamination during the growth interruption, a sample was prepared in the following way. Immediately after growth of a Si buffer layer at high temperature, a 2-nm-thick α-Si layer was deposited at ambient temperature where contamination is most likely. This layer was recrystallized at 650 °C, and a 50-nm-thick Si buffer layer was then deposited at the same temperature. The growth was then interrupted again, and the sample was cooled down to ambient temperature for more than 30 min. Finally, a Si cap layer was grown at 650 °C. No traces of defects or abrupt contrast changes were observed in XTEM images of this sample, indicating that the contrast observed in Fig. 6 was not due to contamination during the interruption of the Si growth. On the other hand, contrast *was* observed, relative to undoped Si separation layers, from Sb bulk modulation-doped layers with a thickness of ~ 100 nm and $N_{Sb} > 5\times10^{19}$ cm^{-3}.

Figure 7 shows a typical high-resolution lattice image of a δ-doped layer prepared using a 250-V accelerated-Sb-ion beam at $T_s = 625$ °C with $N_{Sb}^{2D} = 4.5\times10^{13}$ cm^{-2}. The {111} lattice fringes are continuous and straight across the δ-doped layer, indicating that the layer is coherent, and there is no evidence of Sb precipitation. The width of the dark band is ≤ 2 nm. The estimated foil thickness is ≈ 8 nm, thus there are only ~ 50 Sb atoms in the field of view in Fig. 7. The small number of atoms, distributed randomly within the layer, makes the δ-layer appear less flat than in Fig. 6.

The δ-doped structures were also characterized by diffraction contrast in medium-resolution two-beam and weak-beam images. Figure 8 shows a dark-field XTEM micrograph, imaged using a $\mathbf{g}_{004}$ diffracted beam parallel to the film growth direction, of a series of δ-doped layers in a Si film grown at 620 °C. The δ-doping was done with $V_{Sb} = 200$ V for various doses to provide sheet concentrations from 5.6×10^{12} to 1.5×10^{14} cm^{-2}. Under the two-beam diffraction conditions used, the image is sensitive to strain.[19] As can be seen in the figure, contrast bands, which are continuous and uniform across the sample, are present at positions corresponding to the δ-doped layers, and the contrast increases with increasing Sb sheet doping concentration in the δ-doped layer. These results suggest that the contrast in the XTEM micrographs from δ-doped layers is associated with a strain field. No Sb precipitation was observed, even at the highest concentration studied ($N_{Sb}^{2D} = 1.5\times10^{14}$ cm^{-2}).

Figure 9 is a $\mathbf{g}_{113}$ weak-beam image from the same sample as shown in Fig. 8. Weak-beam images are more sensitive to defects and images obtained using the $\mathbf{g}_{113}$ diffraction vector have been previously shown for $In_xGa_{1-x}As/GaAs$ strained layers to be very sensitive to interfacial topography.[20] In this case, the [110]-oriented cross-sectional foil was tilted $\sim 26°$ towards the [332] pole, in order to view the δ-doped layer along an inclined projection such that intrinsic stresses give rise to fringe contrast. A specimen region with a thickness of ≈ 200

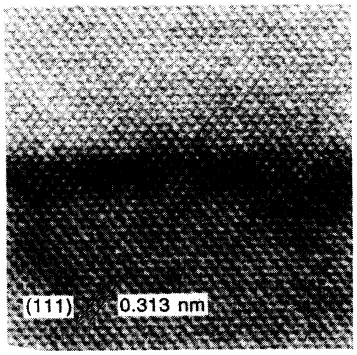

FIG. 7. High-resolution XTEM lattice image of the sample shown in Fig. 6.

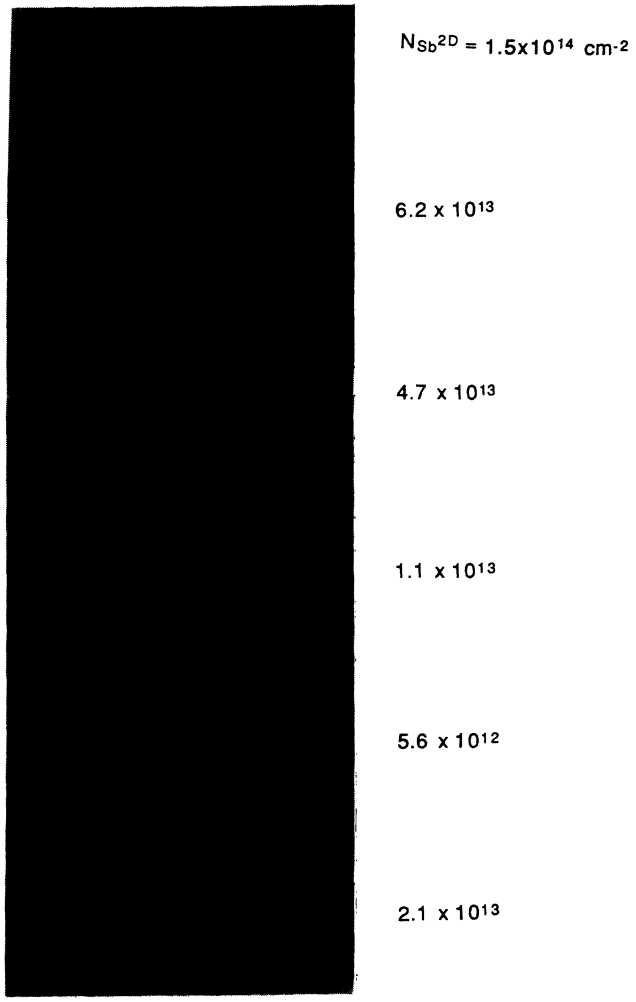

FIG. 8. XTEM two-beam dark-field image of a Sb modulation δ-doped MBE Si film grown with $V_{Sb} = 200$ V and $T_s = 620$ °C. The image was obtained using the $\mathbf{g}_{004}$ diffracted beam. N_{Sb}^{2D} was varied between 5.6×10^{12} and 1.5×10^{14} cm^{-2}.

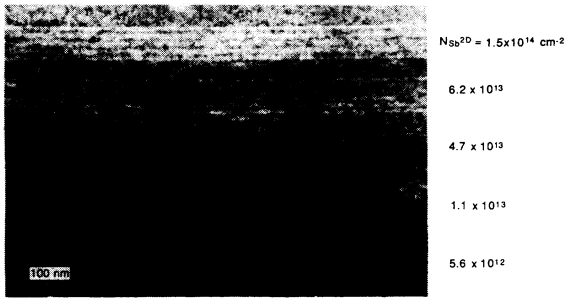

FIG. 9. XTEM g_{113} weak beam image of the same sample shown in Fig. 8.

nm was chosen in order to reveal as many fringes as possible while still maintaining reasonable resolution. As shown in Fig. 9, strain-layer fringes become visible for $N_{Sb}^{2D} \geq 1.1 \times 10^{13}$ cm^{-2}, and the contrast increases with increasing N_{Sb}^{2D}. The lack of contrast variation along the δ-doped layers in Fig. 9 again suggests a uniform distribution of dopant atoms for Sb sheet concentrations up to at least $N_{Sb}^{2D} \approx 1.5 \times 10^{14}$ cm^{-2}.

D. Comparison with SPE δ-doped layers

For comparison, Sb δ-doped layers were also produced using the SPE method. In general, similar contrast-band widths and intensity contrasts were obtained from XTEM images of the two types of samples with similar sheet concentrations. However, the structure and width of δ-doped layers prepared by the SPE method were found to depend on the thickness of the amorphous α-Si layer. Figure 10 shows high-resolution transmission electron microscopy images of SPE Sb δ-doped layers obtained from (a) a 2-nm- and (b) a 4-nm-thick α-Si layer. The widths of the contrast bands shown in Figs. 11(a) and 11(b) correspond to the original α-Si thicknesses, indicating that Sb diffusion through the α-Si layer is faster than

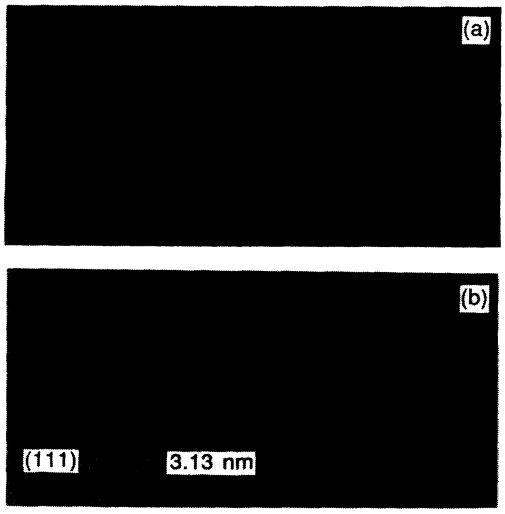

FIG. 10. High-resolution XTEM lattice images of Sb δ-doped layers obtained by SPE with (a) a 2-nm- and (b) a 4-nm-thick amorphous Si cap layer. $N_{Sb}^{2D} = 8 \times 10^{13}$ cm^{-2} and $T_{SPE} = 650$ °C.

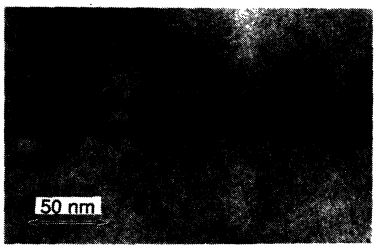

FIG. 11. XTEM g_{004} two-beam dark-field image of a Sb δ-doped layer made by SPE. $N_{Sb}^{2D} = 4 \times 10^{14}$ cm^{-2}, $T_{SPE} = 650$ °C, and the amorphous Si cap-layer thickness = 4 nm. The accumulation of Sb on the recrystallized Si surface due to segregation during crystallization is clearly revealed.

the recrystallization rate.

Strong Sb outdiffusion or segregation through the α-Si layer during recrystallization is more clearly evident in temperature-modulation growth experiments. In this case, a Sb overlayer with a surface coverage $\Theta_{Sb} \approx 4 \times 10^{14}$ cm^{-2} was first deposited at ambient temperature and then the sample was capped with a 20-nm-thick α-Si layer. The amorphous layer was recrystallized at 650 °C, after which the substrate was cooled down to 550 °C for growth of a crystalline Si buffer layer. Since Sb segregation at 550 °C during subsequent growth of the crystalline layer is relatively low, a significant fraction of the Sb atoms will be incorporated at the interface between the recrystallized layer and the buffer layer. This effect is clearly observed in the g_{004} dark-field image in Fig. 11. The contrast band indicates the position of the Sb δ-doped layer. Approximately 20 nm away from this band is a weaker band where Sb atoms were trapped at the interface between the SPE δ-doped layer and the buffer layer after diffusing though the α-Si to the surface during recrystallization.

V. CONCLUSIONS

It has been demonstrated that Sb low-energy ion-beam doping can effectively provide δ-function-shaped doping profiles during Si-MBE growth without requiring post-deposition processing. Analysis by SIMS, *C-V*, and TEM indicate that the widths of the Sb δ-doped regions are only a few atomic layers, in agreement with results from calculations carried out using a recently developed dopant incorporation model. No precipitates or other defects were found in high-resolution XTEM lattice images for Sb δ-doped layers with Sb sheet concentrations $N_{Sb}^{2D} \leq 1.5 \times 10^{14}$ cm^{-2}. The uniformity of the strain in the δ-doped layers prepared by ion-beam doping was confirmed by two-beam and weak-beam XTEM analyses.

ACKNOWLEDGMENTS

We would like to acknowledge useful discussions with Dr. V. Koch at the Technische Universität München, Garching. This work was supported by the Swedish Natural Science Research Council (NFR), the Semiconductor Research Corporation in the U.S. and the U.S. Joint Services Electronics Program.

[1]K. Ploog, J. Cryst. Growth **81**, 304 (1987).
[2]H. P. Zeindl, T. Wegehaupt, I. Eisele, H. Oppolzer, H. Reisinger, G. Tempel, and F. Koch, Appl. Phys. Lett. **50**, 1164 (1987).
[3]H.-M. Li, K.-F. Berggren, W.-X. Ni, B. E. Sernelius, M. Willander, and G. V. Hansson, J. Appl. Phys. **67**, 1962 (1990).
[4]C. E. C. Wood, G. Metze, J. Berry, and L. F. Eastman, J. Appl. Phys. **51**, 383 (1983).
[5]G. Pindoria, R. A. A. Kubiak, S. M. Newstead, and D. P. Woodruff, Surf. Sci. **234**, 17 (1990).
[6]R. A. Metzger and F. G. Allen, J. Appl. Phys. **55**, 931 (1984).
[7]A. A. van Gorkum, K. Nakagawa, and Y. Shiraki, Jpn. J. Appl. Phys. **26**, L1933 (1987).
[8]W.-X. Ni, H.-M. Li, A. Assadi, M. Willander, J.-E. Sundgren, and G. V. Hansson, in *Proceedings of the 13th Nordic Semiconductor Meeting,* edited by M. Östling (The Royal Institute of Technology, Stockholm, 1988).
[9]J.-E. Sundgren, J. Knall, W.-X. Ni, M.-A. Hasan, L. C. Markert, and J. E. Greene, Thin Solid Films **183**, 281 (1989).
[10]W.-X. Ni, J. Knall, M.-A. Hasan, G. V. Hansson, J.-E. Sundgren, S. A. Barnett, L. C. Markert, and J. E. Greene, Phys. Rev. B **40**, 10 449 (1989).
[11]P. Fons, N. Hirashita, L. C. Markert, Y.-W. Kim, J. E. Greene, W.-X. Ni, J. Knall, G. V. Hansson, and J.-E. Sundgren, Appl. Phys. Lett. **53**, 1732 (1988).
[12]W.-X. Ni, H.-M. Li, M. Sardela, M. Willander, J.-E. Sundgren, and G. V. Hansson, in *Proceedings of the 14th Nordic Semiconductor Meeting,* edited by M. Hansen (Institute of Physics, Århus, 1990), p. 215.
[13]L. C. Markert, J. E. Greene, W.-X. Ni, G. V. Hansson, and J.-E. Sundgren, Thin Solid Films **206**, 59 (1991).
[14]J. P. Biersak, Nucl. Instrum. Methods B **27**, 21 (1987).
[15]P. Williams and J. E. Baker, Nucl. Instrum. Methods **182/183**, 15 (1981).
[16]H.-M. Li, W.-X. Ni, M. Willander, K.-F. Berggren, B. E. Sernelius, and G. V. Hansson, Thin Solid Films **183**, 331 (1989).
[17]S. Sze, *Physics of Semiconductor Devices* (Wiley, New York, 1981).
[18]E. F. Schubert and K. Ploog, Jpn. J. Appl. Phys. **25**, 966 (1986).
[19]J. M. Gibson, R. Hull, J. C. Bean, and M. M. J. Treacy, Appl. Phys. Lett. **46**, 649 (1985).
[20]J.-Y. Yao, T. G. Andersson, and G. L. Dunlop, in *Atomic Scale Structure of Interfaces,* edited by R. D. Bringans, R. M. Feenstra, and J. M. Gibson, MRS Symposia Proceedings No. 159 (Materials Research Society, Pittsburgh, 1989), p. 345.

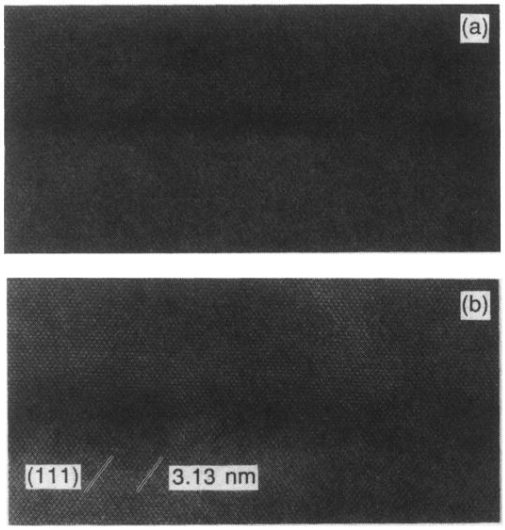

FIG. 10. High-resolution XTEM lattice images of Sb δ-doped layers obtained by SPE with (a) a 2-nm- and (b) a 4-nm-thick amorphous Si cap layer. $N_{\mathrm{Sb}}^{\mathrm{2D}}=8\times10^{13}$ cm^{-2} and $T_{\mathrm{SPE}}=650\,^{\circ}\mathrm{C}$.

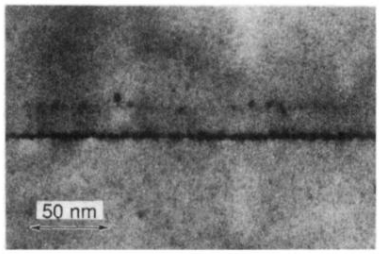

FIG. 11. XTEM $\mathbf{g}_{004}$ two-beam dark-field image of a Sb δ-doped layer made by SPE. $N_{Sb}^{2D}=4\times10^{14}$ cm^{-2}, $T_{SPE}=650$ °C, and the amorphous Si cap-layer thickness = 4 nm. The accumulation of Sb on the recrystallized Si surface due to segregation during crystallization is clearly revealed.

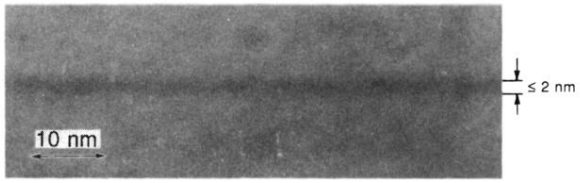

FIG. 6. Bright-field XTEM image of a Sb-ion δ-doped MBE Si(001) layer grown with $V_{Sb}=250$ V and $T_s=625\,^{\circ}\mathrm{C}$. $N_{Sb}^{2D}=5\times10^{13}\ \mathrm{cm}^{-2}$.

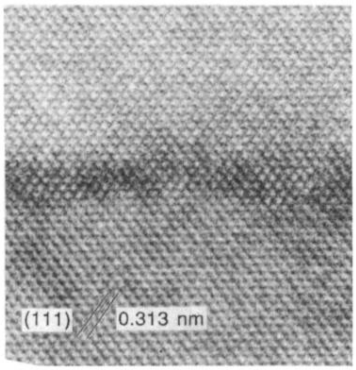

FIG. 7. High-resolution XTEM lattice image of the sample shown in Fig. 6.

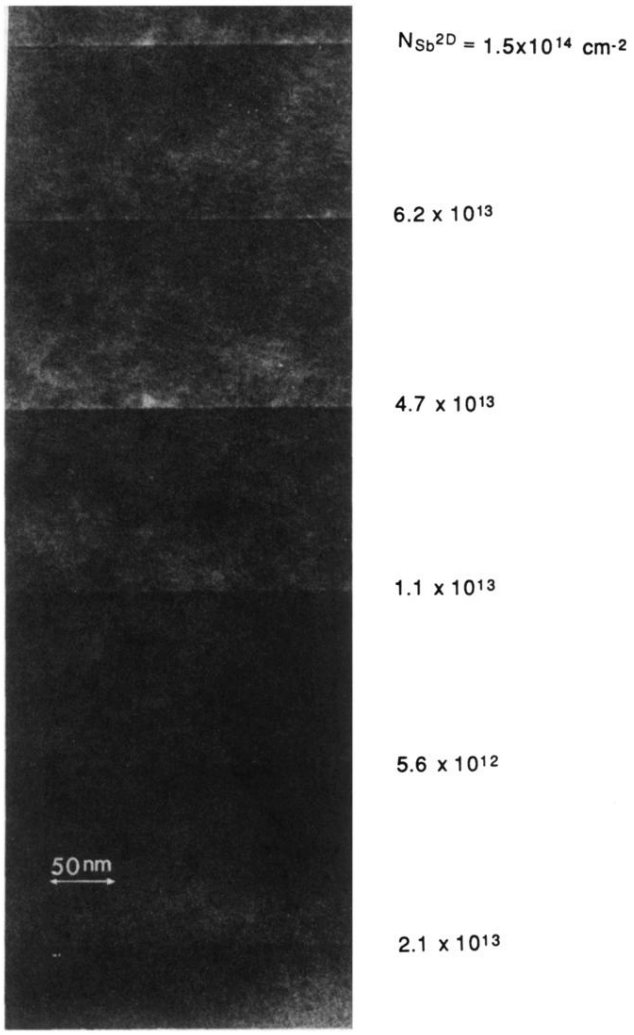

FIG. 8. XTEM two-beam dark-field image of a Sb modulation δ-doped MBE Si film grown with $V_{Sb}=200$ V and $T_s=620$ °C. The image was obtained using the $\mathbf{g}_{004}$ diffracted beam. N_{Sb}^{2D} was varied between 5.6×10^{12} and 1.5×10^{14} cm^{-2}.

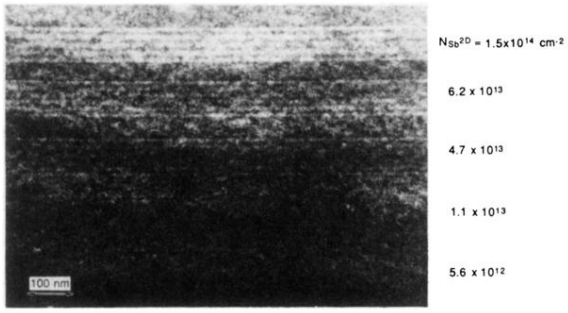

FIG. 9. XTEM $\mathbf{g}_{113}$ weak beam image of the same sample shown in Fig. 8.